Supporting Information

Two-dimensional SnSe Nanonetworks; Growth and Evaluation for Li-ion Battery Applications

*Fionán Davitt[1], Killian Stokes[2], Timothy W. Collins[1], Manuel Roldan-Gutierrez[3], Fred Robinson[4], Hugh Geaney[2], Subhajit Biswas[*1], Shery L.Y. Chang[3], Kevin M Ryan[2], Gillian Reid[4] and Justin D. Holmes[1]*

[1]School of Chemistry & AMBER Centre, University College Cork, Cork, T12 YN60, Ireland. [2]Bernal Institute & Chemical Sciences Department, University of Limerick. [3]Eyring Materials Center and School of Molecular Sciences, Arizona State University, Tempe, AZ 85287, USA

[4]School of Chemistry, University of Southampton, Southampton SO17 1BJ, U.K.

*To whom correspondence should be addressed: Tel: +353 (0)21 4905143; E-mail: s.biswas@ucc.ie (SB)

Experimental

SnSe nanonetworks were synthesised using a liquid-injection CVD method, utilising $[SnCl_4\{^nBuSe(CH_2)_3Se^nBu\}]$ as a single source precursor[1]. This precursor was prepared in the same manner as described in the previous report by de Groot *et. al.* [1] This precursor was dissolved to a concentration of 7.5 mg ml^{-1} in anhydrous toluene, inside a nitrogen filled glovebox, before being loaded in a Hamilton sample-lock Gastight syringe.

The growth of the SnSe nanonetworks was performed on Si (100) substrates without removing the native oxide. For electrochemical testing the samples were grown on stainless steel substrates. Both types of substrates were cleaned in acetone and iso-propyl alcohol (IPA), before being dried with nitrogen and heated in a vacuum oven at 70 °C overnight, to ensure thorough removal of residual moisture. The substrates were then transferred to the CVD chamber with a 6 mm inner diameter quartz tube lining. The growth substrate was placed at the centre of the tube furnace. Prior to precursor injection the chamber was dried under vacuum and purged with high purity argon gas. The reaction chamber was heated to 550 °C, with a constant flow of 1.1 SCCM of argon gas. Injection of the precursor was then initiated and maintained at a constant rate of 1.5 ml h^{-1} using a KDS series 100 single-syringe pump until the desired injection volume was achieved.

Characterisation

After removal from the CVD chamber, the synthesised nanomaterials were analysed using a Zeiss Supra 40 scanning electron microscope (SEM) and a Helios Nanolab 600i SEM. Raman scattering spectroscopy was performed with a Renishaw InVia Raman spectrometer equipped with a 2400 lines/mm grating using a 514 nm laser. Spectra were collected using a RenCam CCD camera, with the beam focused onto the samples using a 50× objective lens. Measurements were undertaken at 1% of the total 1.9 mW laser power. The crystal structure of the product was confirmed by X-ray diffraction (XRD) using a Philips X'pert Pro MPD equipped with a Panalytical Empyrean Cu X-ray tube and a Philips X'celerator detector. The products were mechanically removed from the Si growth substrate for (scanning) transmission electron microscopy ((S)TEM) and energy dispersive X-ray (EDX) analysis. Removal of the nanomaterial was easily achieved through a quick sonication of the growth substrate in an ultrasonic bath, using a small amount of IPA. The resulting solution was then drop-cast onto a carbon-coated TEM grid. TEM analysis was performed on a JEOL 2100 electron microscope operating at 200 kV and an FEI Titan electron microscope operating at 300 kV. STEM and EDX

analysis were performed on an FEI Titan electron microscope operating at 300 kV. High annular dark field (HAADF) and bright field (BF) STEM imaging, EDX mapping and Electron energy loss spectroscopy (EELS) was performed on a Probe Corrected JEOL ARM TEM operating at 200 kV.

Electrochemical testing was carried out galvanostatically using a Biologic MPG-2. The two electrode Swagelok type half-cells were assembled within an Ar filled glovebox with H_2O and O_2 levels below 1 ppm. The SnSe samples were directly grown on stainless steel current collectors and tested as the working electrode versus a Li metal counter/reference electrode. Typical areal loadings for the samples were ~0.2 mg/cm^2. All potentials mentioned are quoted relative to Li/Li$^+$. Celgard separators impregnated with a carbonate based electrolyte (1.0 M lithium hexafluorophosphate ($LiPF_6$) solution in ethylene carbonate and diethyl carbonate, battery grade Aldrich) with 3 wt% vinylene carbonate (97 % purity, Aldrich) were used. A specific current of ± 100 mAh g^{-1} was applied for testing within a cycling window of 3.0 - 0.011 V (vs. Li/Li$^+$) to fully include the alloying and conversion processes. The mass of the SnSe active material was determined through careful measurement using a Sartorius Ultra-Microbalance SE2 (repeatability ± 0.25 μg). Thorough accurate weighing at each stage in electrode preparation ensured accurate mass loadings which were used to calculate the C rate and galvanostatic capacities.

Author (Year)	Material	Number of Cycles	Initial Discharge Capacity (mAh/g)	Final Discharge Capacity (mAh/g)	Capacity retention (%)
Xue, M.-Z.; et al. (2006)[2]	SnSe Thinfilm	60	681	>100	15
Ning, J.; et al. (2011)[3]	SnSe/carbon black/poly-vinylidenefluoride	30	353	~200	~56.7
Kang, S. Z.; et al. (2012)[4]	SnSe nanosheets/ poly(vinylidene fluoride)/carbon black	20	1009	73	7.2
Wang, X; et al. (2014)[5]	SnSe nanocrystal/carbon fabric	80	1216	676	55.6
Im, H.S.; et al. (2014)[6]	SnSe, $SnSe_2$, GeSe, $GeSe_2$	70	867 (SnSe), 647 (SnSe2), 1232 (GeSe), 1099 (GeSe2)	510 (SnSe), 412 ($SnSe_2$), 771 (GeSe), 514 ($GeSe_2$)	58.8 (SnSe), 63.7 ($SnSe_2$), 62.6 (GeSe), 46.8 ($GeSe_2$)
Zhang, Z.; et al. (2015)[7]	SnSe/carbon nanocomposite	100	1097.6	633.1	57.7
Gurung, A; et al. (2016)[8]	SnSe/multi-walled carbon nanotubes	50	1241	651	52.5
Zhang, L; et al. (2016)[9]	SnSe/carbon composite	100	1148	840	73.2
Wang, D; et al. (2016)[10]	SnSe nanorods/graphene oxide	100	1362	764	56
Wang, W.; et al. (2017)[11]	Layered SnSe Nanoplates	300	~1190	787.9	66.2
Lee, D.-H.; et al. (2017)[12]	SnSe/C	200	726	626	86.2
Cheng, Y.; et al. (2019)[13]	SnSe, SnSe/r-GO Composite	150 (SnSe) 200 (SnSe/r-GO)	1302 (SnSe) 1049 (SnSe/r-GO)	<300 (SnSe) 1002 (SnSe/r-GO)	<23 (SnSe) 95.5 (SnSe/r-GO)
This Work	SnSe nanonetworks	50	1043	959	92

Table S1. Comparison of the performance for previously published SnSe anodes

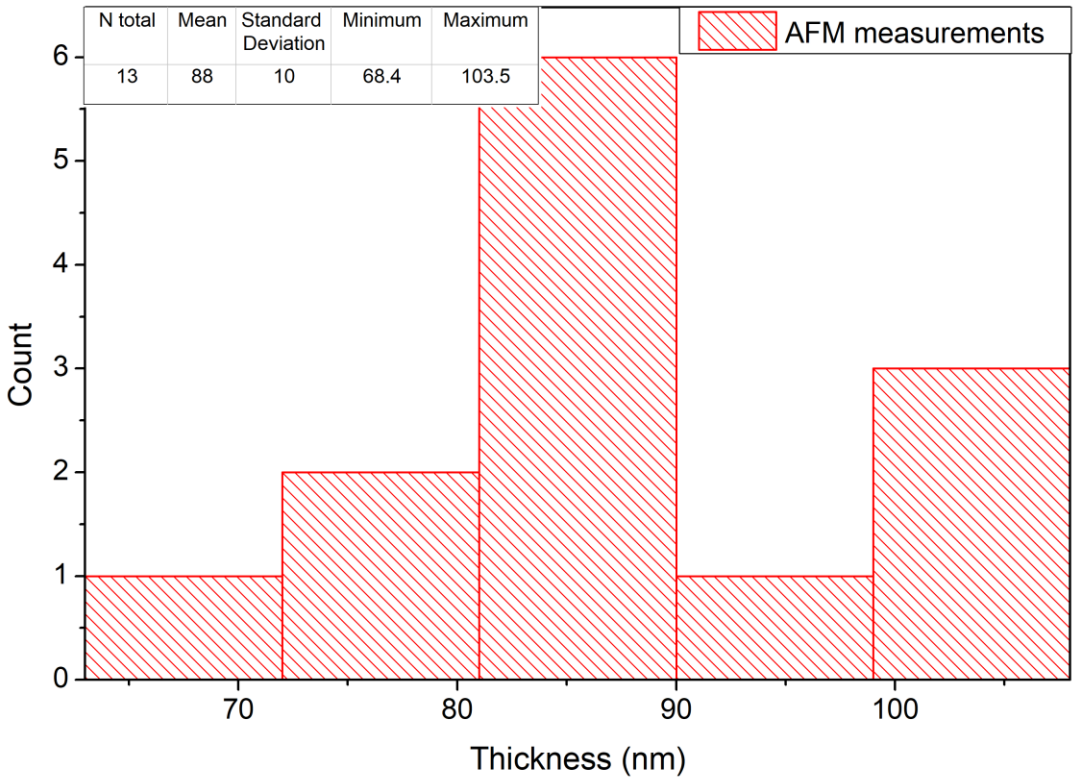

Figure S1: Histogram of AFM thickness measurements at various points of the SnSe nanonetworks.

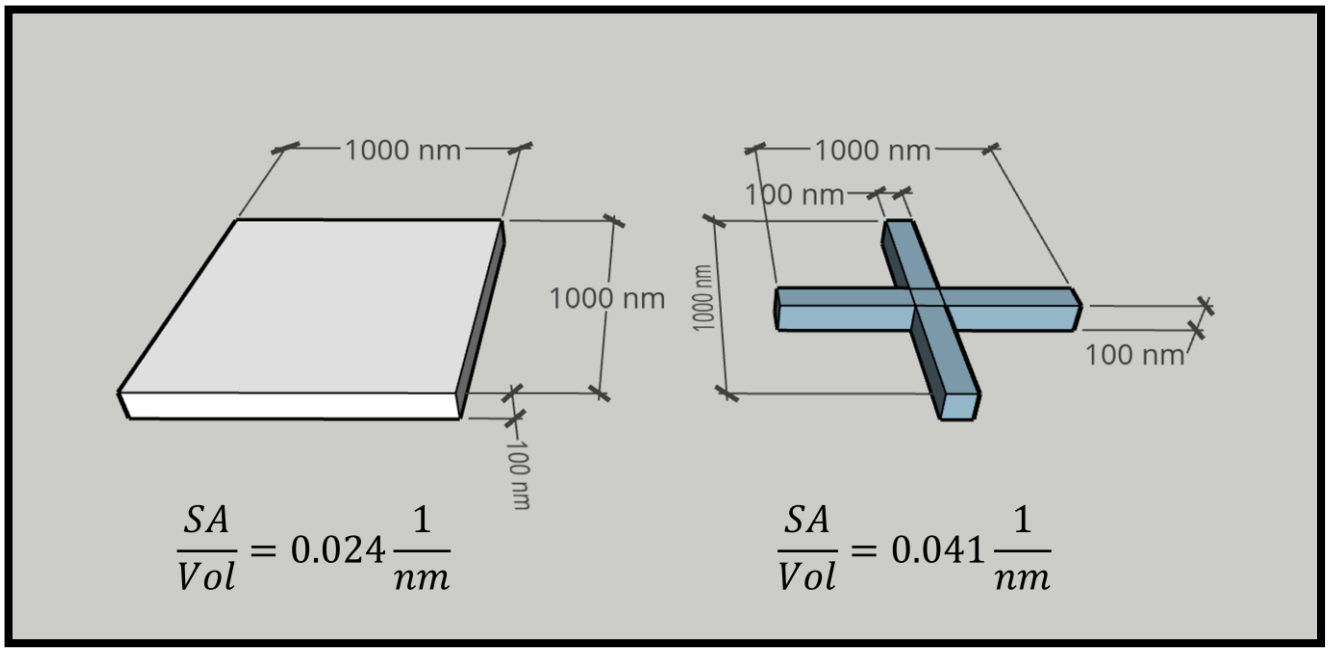

Figure S2: Surface area to volume ratio comparison for a uniform flake structure compared to a networked structure. Network structures present a higher surface area to volume ratio.

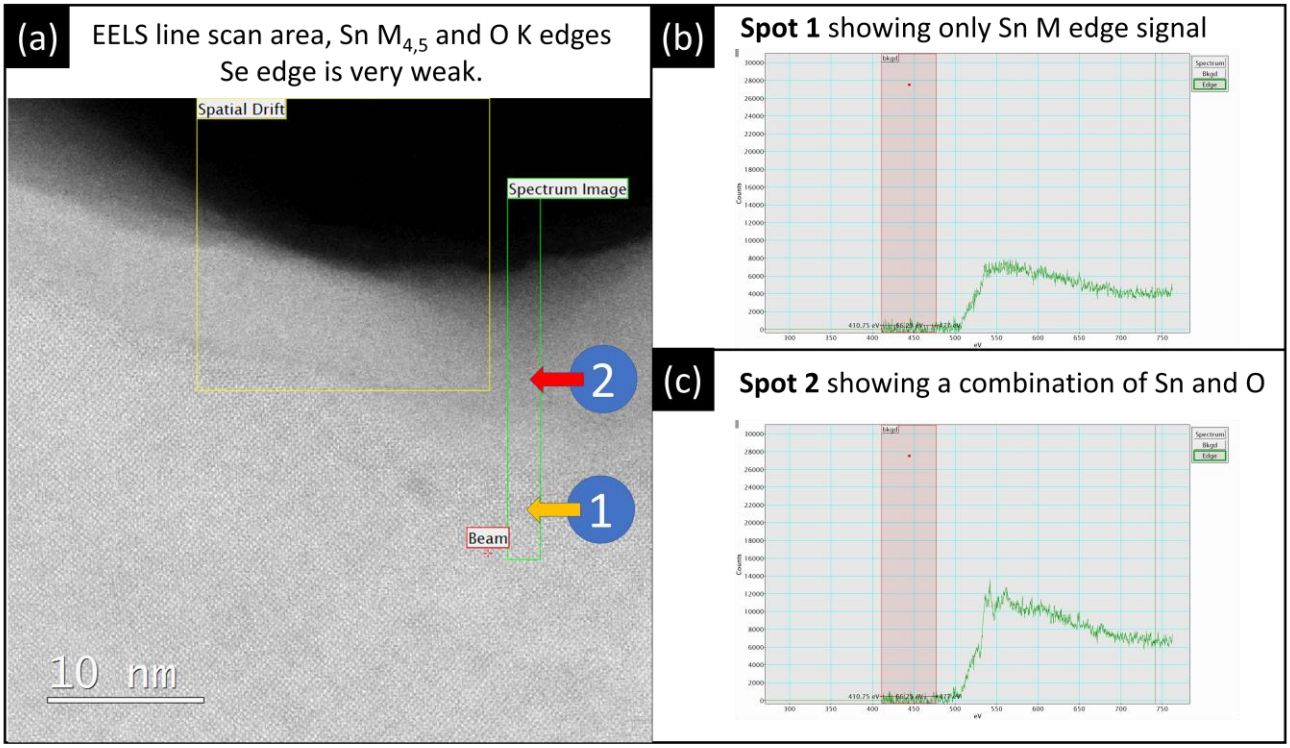

Figure S3: EELS Sn and O analysis of the surface of a SnSe nanonetwork. The first 5-10 nm layer at the surface is composed of SnO_x.

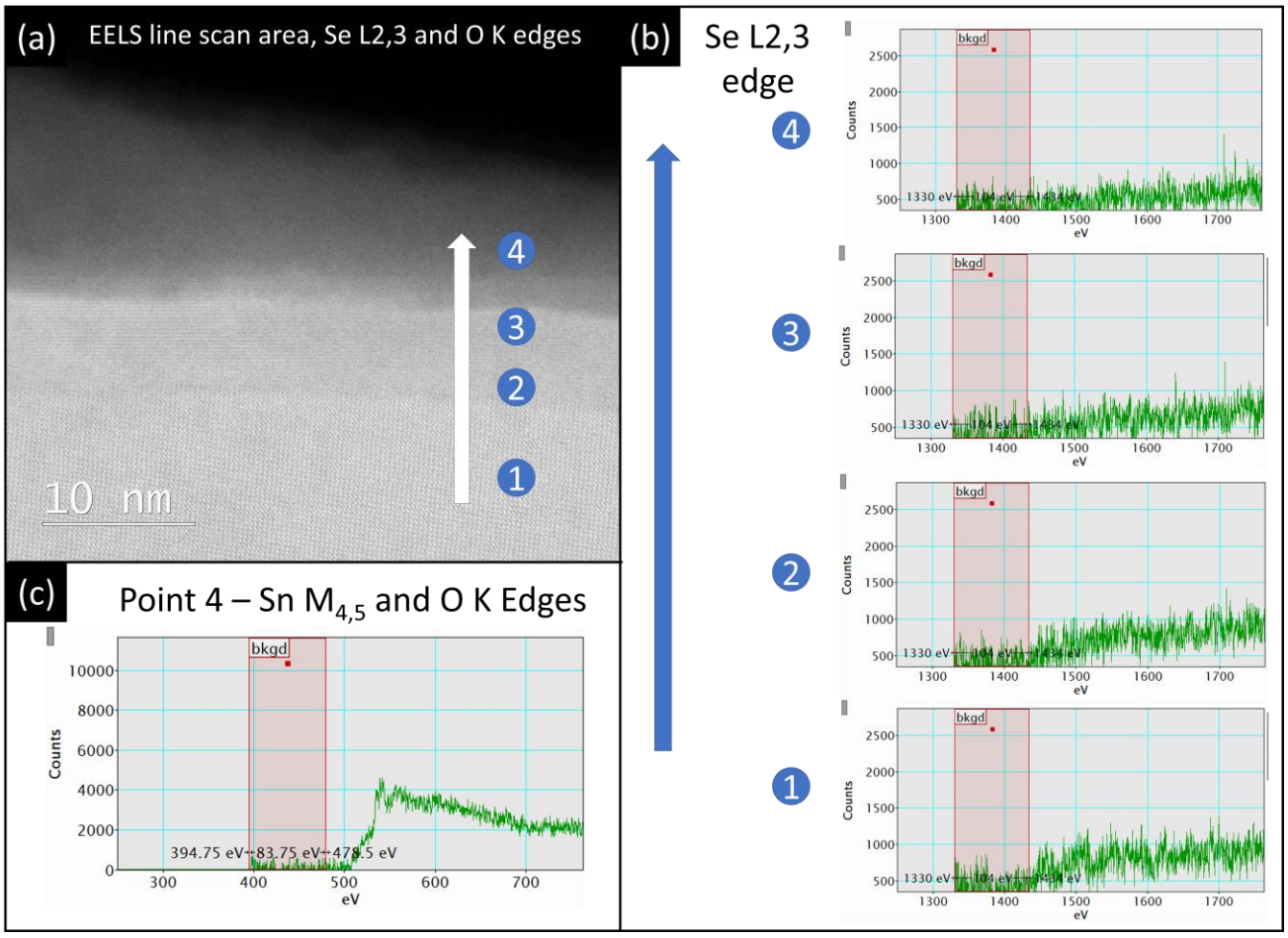

Figure S4: EELS Se and O analysis of the surface of a SnSe nanonetwork. (a) shows a STEM image of a section of the SnSe nanonetwork. The spots labelled 1 to 4, indicate where the EELS measurements in (b) are taken from. A decreasing Se signal is seen moving from spot 1 to 3, which then vanishes in region 4. (c) shows that the outmost surface at region 4 shows only a SnO_x signal.

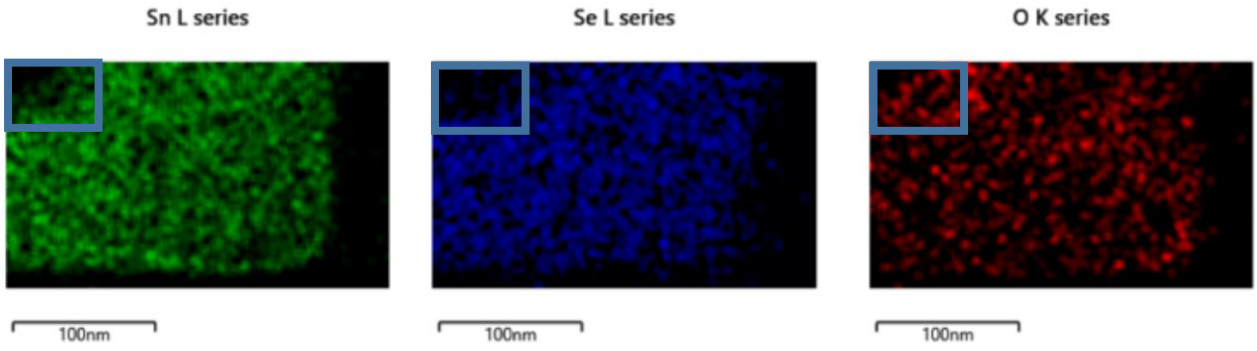

Figure S5: EDX mapping of a section of the SnSe network. The blue box is included as a guide for the eye, highlighting the surface region at a junction in the network. The surface is seen to consist of Sn and O, with depleted Se at the outermost surface.

.

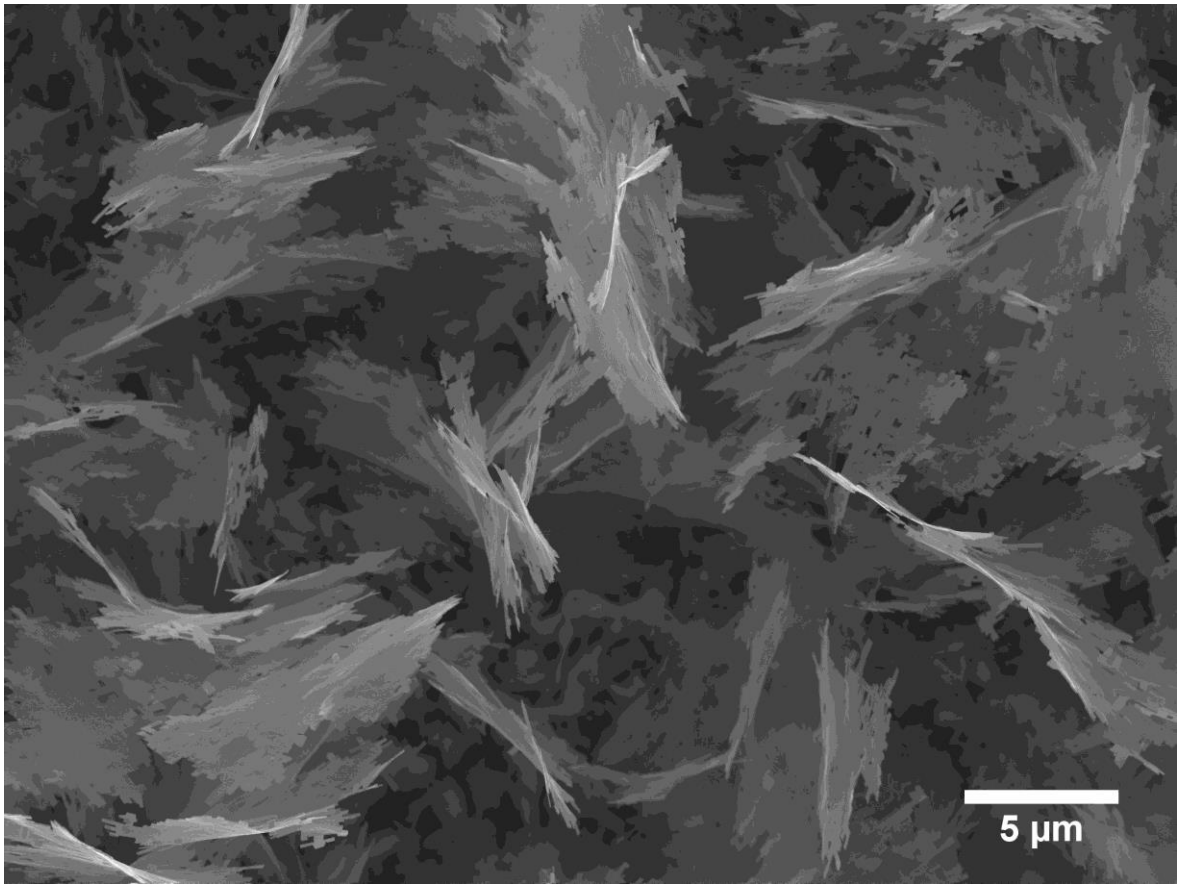

Figure S6: Growth of the SnSe nanonetworks on a stainless steel substrate.

References:

(1) De Groot, C. H.; Gurnani, C.; Hector, A. L.; Huang, R.; Jura, M.; Levason, W.; Reid, G. Highly Selective Chemical Vapor Deposition of Tin Diselenide Thin Films onto Patterned Substrates via Single Source Diselenoether Precursors. *Chem. Mater.* **2012**, *24*, 4442–4449.

(2) Xue, M. Z.; Yao, J.; Cheng, S. C.; Fu, Z. W. Lithium Electrochemistry of a Novel SnSe Thin-Film Anode. *J. Electrochem. Soc.* **2006**, *153*, 270–274.

(3) Ning, J.; Xiao, G.; Jiang, T.; Wang, L.; Dai, Q.; Zou, B.; Liu, B.; Wei, Y.; Chen, G.; Zou, G. Shape and Size Controlled Synthesis and Properties of Colloidal IV–VI SnSe Nanocrystals. *CrystEngComm* **2011**, *13*, 4161.

(4) Kang, S. Z.; Jia, L.; Li, X.; Yin, Y.; Li, L.; Guo, Y. G.; Mu, J. Amine-Free Preparation of SnSe Nanosheets with High Crystallinity and Their Lithium Storage Properties. *Colloids Surfaces A Physicochem. Eng. Asp.* **2012**, *406*, 1–5.

(5) Wang, X.; Liu, B.; Xiang, Q.; Wang, Q.; Hou, X.; Chen, D.; Shen, G. Spray-Painted Binder-Free SnSe Electrodes for High-Performance Energy-Storage Devices. *ChemSusChem* **2014**, *7*, 308–313.

(6) Im, H. S.; Lim, Y. R.; Cho, Y. J.; Park, J.; Cha, E. H.; Kang, H. S. Germanium and Tin Selenide Nanocrystals for High-Capacity Lithium Ion Batteries: Comparative Phase Conversion of Germanium and Tin. *J. Phys. Chem. C* **2014**, *118*, 21884–21888.

(7) Zhang, Z.; Zhao, X.; Li, J. SnSe/Carbon Nanocomposite Synthesized by High Energy Ball Milling as an Anode Material for Sodium-Ion and Lithium-Ion Batteries. *Electrochim. Acta* **2015**, *176*, 1296–1301.

(8) Gurung, A.; Naderi, R.; Vaagensmith, B.; Varnekar, G.; Zhou, Z.; Elbohy, H.; Qiao, Q. Tin Selenide – Multi-Walled Carbon Nanotubes Hybrid Anodes for High Performance Lithium-Ion Batteries. *Electrochim. Acta* **2016**, *211*, 720–725.

(9) Zhang, L.; Lu, L.; Zhang, D.; Hu, W.; Wang, N.; Xu, B.; Li, Y.; Zeng, H. Dual-Buffered SnSe@CNFs as Negative Electrode with Outstanding Lithium Storage Performance. *Electrochim. Acta* **2016**, *209*, 423–429.

(10) Wang, D.; Zhang, K.; Zhu, Y.; Lan, Y.; Hu, L.; Lin, N.; Zhou, J.; Qian, Y. A Novel Strategy to Prepare Graphene Oxide-Wrapped Nanocrystals Composite for High-Performance Lithium Storage. *Mater. Lett.* **2016**, *175*, 32–35.

(11) Wang, W.; Li, P.; Zheng, H.; Liu, Q.; Lv, F.; Wu, J.; Wang, H.; Guo, S. Ultrathin Layered SnSe Nanoplates for Low Voltage, High-Rate, and Long-Life Alkali–Ion Batteries. *Small* **2017**, *13*, 1–7.

(12) Lee, D.-H.; Park, C.-M. Tin Selenides with Layered Crystal Structures for Li-Ion Batteries: Interesting Phase Change Mechanisms and Outstanding Electrochemical Behaviors. *ACS Appl. Mater. Interfaces* **2017**, *9*, 15439–15448.

(13) Cheng, Y.; Huang, J.; Li, J.; Cao, L.; Xu, Z.; Luo, X.; Qi, H.; Guo, P. SnSe/r-GO Composite with Enhanced Pseudocapacitance as a High-Performance Anode for Li-Ion Batteries. *ACS Sustain. Chem. Eng.* **2019**, *7*, 8637–8646.